ties might result in shorter necks, which can be represented by a larger α. These effects would result in smearing of the transitions between the quantized levels in Fig. 3. Probing a strongly smeared conductance curve at discrete values of the contact area will show little sign of the quantization, but may produce peaks in the histogram corresponding to stable atomic geometries. Indeed, there are reproducible peaks near 1.6, 2.4, 3.4 and 4.2 G_0 (Fig. 2*b*) and we speculate that these are due to preferred atomic configurations of the copper contact.

Our experiments show that the variation of the conductance in atomic-scale metal contacts of varying size is therefore determined both by quantization of the conductance and by the discreteness of the contact size. The characteristic sequence of quantum numbers observed in the conductance histogram for sodium gives compelling evidence for the dominant presence of quantized conductance channels, which is explained by its free-electron properties, and is only observable after averaging over a large number of atomic geometries. Even for a *d*-metal such as copper, the quantization pattern can be recognized in the lower range of the conductance, but the role of atomic geometries is more prominent. Having observed quantization of the conductance, it is of interest to study the effect of these quantum-size phenomena on other physical properties, such as magnetic impurity scattering and superconductivity. Such experiments are already being performed[17,18]. □

Received 24 January; accepted 1 June 1995.

1. Beenakker, C. W. J. & van Houten, H. in *Solid State Physics* Vol. 44 (eds Ehrenreich, H. & Turnbull, D.) (Academic, New York, 1991).
2. van Wees, B. J. *et al. Phys. Rev. Lett.* **60,** 848–850 (1988).
3. Wharam, D. A. *et al. J. Phys.* C**21,** L209–L214 (1988).
4. Bogachek, É. N., Zagoskin, A. N. & Kulik, I. O. *Soviet J. Low Temp. Phys.* **16,** 796–800 (1990).
5. Torres, J. A., Pascual, J. I. & Sáenz, J. J. *Phys. Rev.* B**49,** 16581–16584 (1994).
6. Krans, J. M. *et al. Phys. Rev.* B**48,** 14721–14724 (1993).
7. Agraït, N., Rodrigo, J. G. & Vieira, S. *Phys. Rev.* B**47,** 12345–12348 (1993).
8. Olesen, L. *et al. Phys. Rev. Lett.* **72,** 2251–2254 (1994).
9. Pascual, J. I. *et al. Phys. Rev. Lett.* **71,** 1852–1855 (1993).
10. Olesen, L. *et al. Phys. Rev. Lett.* **74,** 2147 (1995).
11. Krans, J. M. *et al. Phys. Rev. Lett.* **74,** 2146 (1995).
12. Muller, C. J., van Ruitenbeek, J. M. & de Jongh, L. J. *Physica* C**191,** 485–504 (1992).
13. Muller, C. J., van Ruitenbeek, J. M. & de Jongh, L. J. *Phys. Rev. Lett.* **69,** 140–143 (1992).
14. Krans, J. M. & van Ruitenbeek, J. M. *Phys. Rev.* B**50,** 17659–17661 (1994).
15. Agraït, N., Rodrigo, J. G., Sirvent, C. & Vieira, S. *Phys. Rev.* B**48,** 8499–8501 (1993).
16. de Heer, W. A. *Rev. mod. Phys.* **65,** 611–676 (1993).
17. Yanson, I. K. *et al. Phys. Rev. Lett.* **74,** 302–305 (1995).
18. van der Post, N., Peters, E. T., Yanson, I. K. & van Ruitenbeek, J. M. *Phys. Rev. Lett.* **73,** 2611–2613 (1994).

ACKNOWLEDGEMENTS. We thank C. W. J. Beenakker, C. J. Muller, A. P. Sutton and T. N. Todorov for stimulating discussions. This work was supported by the 'Nederlandse organisatie voor Wetenschappelijk Onderzoek' (NWO) as part of the research collaboration programme between the Ukraine and the Netherlands, and by the 'Stichting voor Fundamenteel Onderzoek der Materie' (FOM).

Synthesis and characterization of carbide nanorods

Hongjie Dai, Eric W. Wong, Yuan Z. Lu, Shoushan Fan & Charles M. Lieber*

Department of Chemistry and Division of Applied Sciences, Harvard University, Cambridge, Massachusetts 02138, USA

THE properties and potential applications of carbon nanotubes filled with other materials have aroused much speculation[1–5]. Strategies for filling nanotubes include *in situ* growth in an arc reactor using metal/carbon composites[2,5] and the capillarity-driven filling of open nanotubes using liquid reagents[3,4]. Here we report an alternative approach to the synthesis of nanoscale structures based on nanotubes, in which the tubes are converted to carbide rods by reaction with volatile oxide and/or halide species. In this way we have been able to prepare solid carbide nanoscale rods of TiC, NbC, Fe_3C, SiC and BC_x in high yield with typical diameters of between 2 and 30 nm and lengths of up to 20 μm. Preliminary studies show that these rods share the properties of the bulk materials (such as magnetism and superconductivity), suggesting that they might allow the investigation of the effects of confinement and reduced dimensionality on such solid-state properties. These carbide nanorods might also find technological applications in nanostructured composite materials.

Our preparation of carbide nanorods involves the reaction of carbon nanotubes with volatile metal or non-metal complexes (Fig. 1). The carbon nanotubes used in these vapour–solid reactions were obtained from metal-catalysed growth using ethylene and hydrogen[6]. This procedure yields relatively pure nanotube samples compared with arc-discharge methods[7–9], although the nanotubes exhibit poor crystallinity (Fig. 2*a*). Previous studies have also shown that SiO vapour can be used to convert carbon fibres[10] and nanotubes[11] to SiC rods, although the sizes of these SiC products were typically much larger than the carbon precursor[11]. In our studies discussed below, the diameters of the solid nanorods are similar to the starting diameters of the nanotube reactants and significantly smaller than reported previously[10,11]. Furthermore, our general approach (Fig. 1) has been exploited to prepare a wide range of chemically distinct carbide materials.

The morphology and structure of the products obtained from the reaction of TiO and carbon nanotubes at 1,375 °C are shown in Fig. 2. Transmission electron microscopy (TEM) images of the reaction product (Fig. 2*b–d*) show both straight and smoothly curved, solid rod-like structures that are distinct from the irregularly curved and hollow carbon nanotube reactant (Fig. 2*a*). These images also show that the diameters of the rod-like products are similar to that of the carbon nanotubes, 2–30 nm, and that the lengths typically exceed 1 μm. Energy dispersive X-ray fluorescence and electron energy-loss spectroscopy measurements demonstrate that these nanorods contain only titanium and sp^3-hybridized carbon, and thus are consistent with the conversion of the carbon nanotubes into titanium carbide (TiC).

This formulation is further established by structural analyses. Powder X-ray diffraction (XRD) measurements on nanorod samples produced using either TiO or $Ti + I_2$ show diffraction peaks that can be indexed to the known cubic, rock-salt structure of TiC with no evidence of either graphitic (nanotube), Ti-metal or Ti-oxide peaks present. The measured lattice constant, $a = 4.326$ Å, is consistent with a stoichiometry TiC_x, with $x \approx 1$ (ref. 12). TEM and electron diffraction studies of single nano-

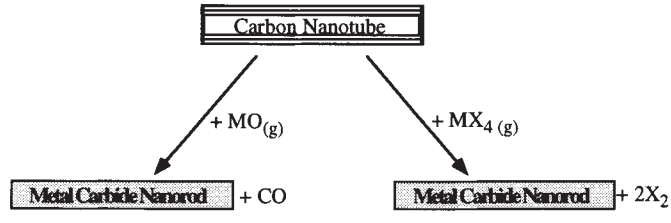

MO = volatile metal or non-metal oxide
MX_4 = volatile metal or non-metal halide

FIG. 1 Reaction scheme used to prepare metal carbide nanorods.

* To whom correspondence should be addressed.

rods (Fig. 2*c–f*) provide further insight into the structures of these TiC materials. In general, we observe smooth (Fig. 2*c*), regular saw-tooth (Fig. 2*d*) and irregularly faceted (Fig. 2*e*) nanorod morphologies; the TiC nanorods also appear to be single crystals with a very low density of stacking faults. Convergent beam electron diffraction patterns recorded along the ⟨111⟩ zone axis perpendicular to the axis of the smooth nanorod (Fig. 2*c*) exhibit a lattice constant and six-fold symmetry corresponding to the (111) planes of cubic TiC. These data imply that the axis of the smooth TiC nanorods is [110]. Similar studies of the saw-tooth nanorod (Fig. 2*d*) demonstrate that the rod axis is also [110] for this morphology. The [110] direction is not unique for the TiC nanorods. In the irregularly faceted nanorods (Fig. 2*e*,*f*), high-resolution TEM and electron diffraction demonstrate that the rod axis is [111], and further show that the TiC nanorods contain single-crystal domains often exceeding 1 μm in length. We note that the saw-tooth morphology has obvious advantages for some applications (for example, composites), although more work is clearly needed to understand and control its growth.

Our approach to carbide nanorod synthesis seems to be general. For example, structural and composition analyses of the material produced from the reaction of carbon nanotubes with Si and I_2 are consistent with the formation of silicon carbide (SiC) nanorods. TEM images show that the SiC nanorods produced from this reaction are relatively straight, solid rods (Fig. 3*a*, *b*). The diameters of the SiC rods produced in the $Si + I_2$ reaction at 1,200 °C are typically 2–20 nm (similar to the diameters of the carbon nanotube reactants), and have lengths of the order of 1 μm. These diameters are significantly smaller than reported[11] recently for the reaction of SiO with impure nanotubes at 1,700 °C. X-ray diffraction patterns from bulk samples were indexed to the zinc blende β-SiC structure and show no evidence of other crystalline impurities. Transmission electron microscopy shows that these SiC nanorods possess a high density of planar defects (Fig. 3*b–d*) in contrast to the near-single-crystal TiC nanorods. We suggest that the defects in [111] oriented rods (Fig. 3*b*, *d*) are rotational twin stacking faults, by analogy with previous observations made on larger SiC whiskers[13,14]. The rod axes lie along the [111] direction in all of the nanorods prepared at 1,300–1,400 °C using SiO as the volatile silicon reactant, but at the lower $Si + I_2$ reaction temperatures (1,100–1,200 °C) this direction is not unique. A high-resolution TEM image of one 7-nm-diameter SiC nanorod (Fig. 3*c*) produced at 1,200 °C shows that the rod axis lies along the [100] direction, although small defect regions with a [111] direction are also present.

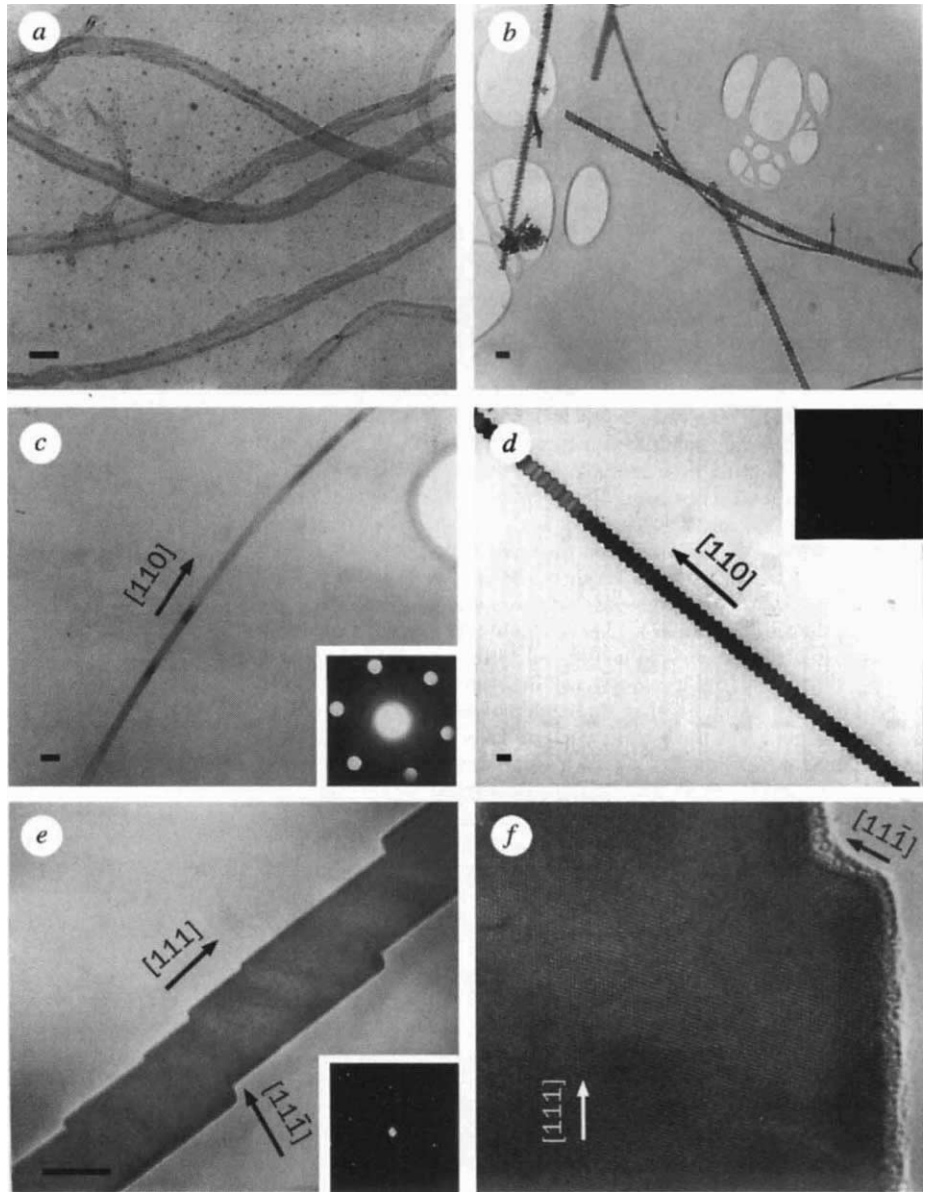

FIG. 2 TEM images of carbon nanotubes (*a*) and TiC nanorods (*b–f*). The nanotubes are imaged as irregular dark lines with light (hollow) centres, whereas the nanorods appear uniform (solid) across the rod axis. Low-resolution images (*b*) show that the nanorods grow with smooth and rough morphologies. The rod axes for these different morphologies were determined from electron diffraction and high-resolution images of single nanorods and are indicated with arrows in the images *c–f*. The regular sawtooth morphology (*d*) has a [110] rod axis and a sawtooth angle of 109°. The irregular facets seen in the rods with a [111] axis (*e*) were found in high-resolution lattice plane images (*f*) to lie along the [11$\bar{1}$] direction. Variations in contrast seen along the nanorod axes (*b–d*) are due to orientation variations of the nanorods on the TEM supports. The insets in *c–e* correspond to electron diffraction patterns recorded along zone axes perpendicular to the rod axes (see text). The scale bars in *a–e* correspond to 20 nm. The carbon nanotubes were grown at 760 °C using an ethylene/hydrogen feedstock and a supported iron catalyst[6]. The TiC nanorods were obtained from the reaction of carbon nanotubes and TiO at 1,375 °C for 12 h. The nanorods were easily dispersed in organic solvents, unlike carbon nanotubes[9].

TABLE 1 Summary of the structure and properties of carbide nanorods

Carbide nanorod	Metal reactant* (reaction temp., °C)	Nanorod structure†	Properties‡
TiC	TiO (1,300–1,400) $Ti + I_2$ (1,200–1,300)	Single crystal	Metal
NbC	$Nb + I_2$ ($\geqslant$700)	Polycrystalline	Superconductor
Fe_3C	$FeCl_3$ (1,350)	Amorphous	Ferromagnetic
SiC	$Si + I_2$ (1,100–1,200) SiO (1,300–1,450)	Single crystal	Semiconductor
BC_x	B_2O_2 (1,400)	Polycrystalline	Insulator

* All reactions (except for the case of boron carbide) were carried out in quartz tubes sealed under vacuum with the carbon nanotubes and metal reactants spatially separated. Boron carbide was formed in a flow reactor (Ar carrier) with B_2O_2 generated *in situ* by the reaction of boron with TiO_2[19]. Titanium was not detected in the resulting boron carbide nanorods. Phases were identified from structure and composition data. For the boron carbide nanorods, the data was most consistent with $B_{13}C_2$, although solid B_4C cannot be ruled out.

† The physical dimensions of the nanorods were similar: diameters of 2–30 nm and lengths typically >1 μm.

‡ The superconducting ($T_c \approx 9$ K; superconducting fraction ~70%) and ferromagnetic character of the NbC and Fe_3C nanorods were determined directly from d.c. magnetization measurements. The bulk T_c of NbC is ~12 K. The properties of the TiC, SiC and BC_x nanorods are inferred from the bulk materials.

Results from the synthesis of other metal carbides using our approach are summarized in Table 1. For example, the reaction of Nb metal and I_2 with carbon nanotubes yields NbC nanorods (Fig. 3*e*, *f*). X-ray diffraction data show that this reaction results in the complete conversion of the nanotubes into the cubic, rock-salt phase of NbC. TEM images and selected-area electron diffraction show that the NbC nanorods produced in these reactions are polycrystalline with morphologies (Fig. 3*e*, *f*) similar to the carbon nanotube starting materials. Significantly, these polycrystalline nanorods are also found to be superconducting, as is bulk NbC (see Table 1). The polycrystalline structure is probably due to the relatively low reaction temperature (730 °C), and thus it should be possible in the future to optimize the growth conditions and produce single-crystal NbC nanorods. The present reaction conditions can, however, yield unique morphologies, such as helical nanorods (Fig. 3*f*), that may also exhibit novel properties. These helical nanorods are believed to result from a direct conversion of helical carbon nanotubes produced in the catalytic growth process. Preliminary reactions between carbon nanotubes and $FeCl_3$ have been found to yield ferromagnetic Fe_3C nanorods (Table 1). Although these materials appear to be amorphous, we believe that the results are significant because the nanorods are magnetic.

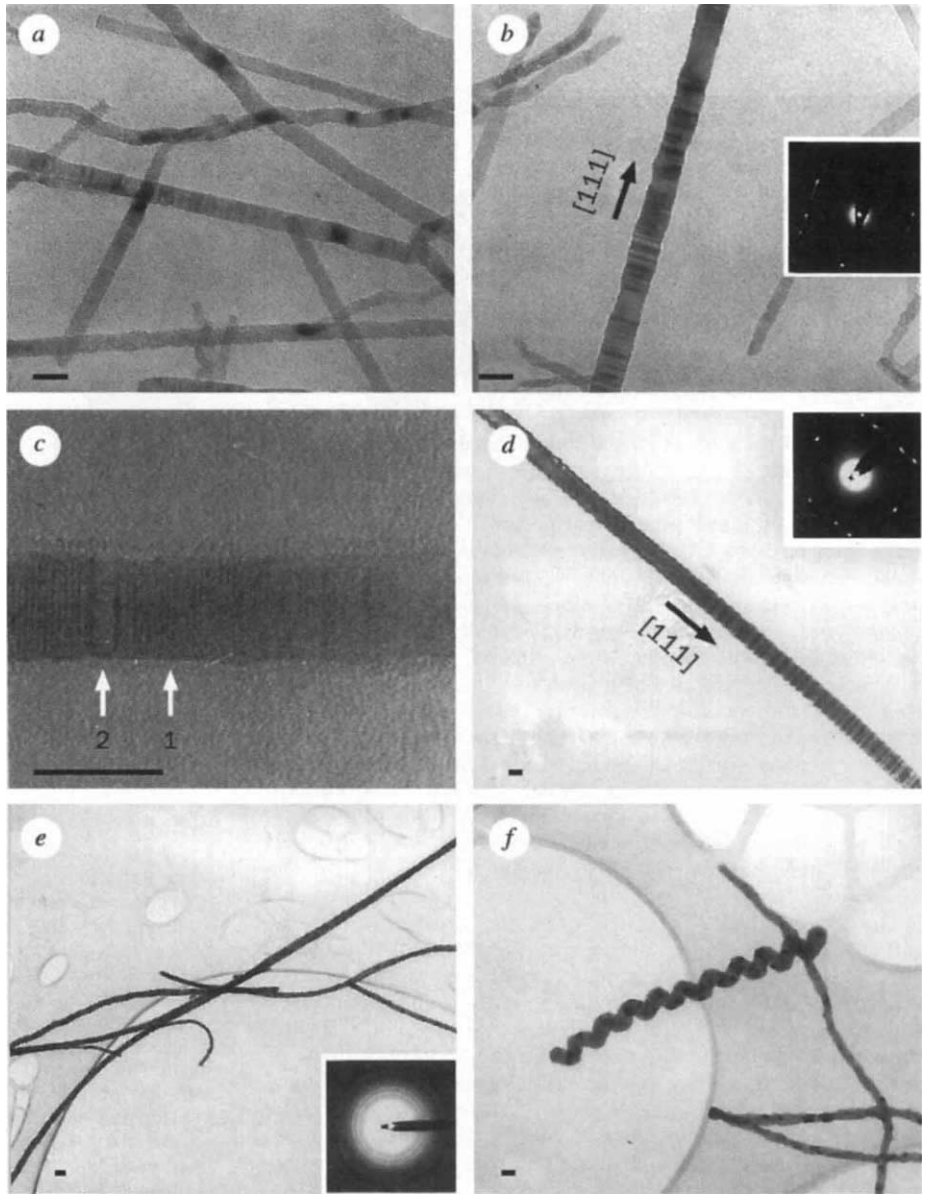

FIG. 3 TEM images of SiC nanorods (*a–d*) and NbC nanorods (*e–f*). The SiC nanorods exhibit a high density of striations, which correspond to stacking faults, perpendicular to the rod axes. Selected area electron diffraction patterns recorded on samples with striations perpendicular to the [111] direction (*b*, *d*) exhibit extra diffraction spots along the ⟨110⟩ zone axis that are characteristic of twinning[13,14]. A high-resolution lattice image (*c*) also shows a SiC nanorod with a primary rod axis direction of [100] (region labelled '1') and growth defects consisting of several unit cells oriented along [111] (region 2). The small dark and light regions in the NbC samples (*e*, *f*) correspond to individual crystal grains in these polycrystalline nanorods. The insets in *b* and *d* correspond to electron diffraction patterns recorded along zone axes perpendicular to the rod axes. Selected area diffraction of the NbC (inset e) shows a ring structure characteristic of a polycrystalline sample; the diffraction pattern was indexed to pure cubic NbC. The scale bars in *a*, *b* and *d–f* correspond to 20 nm; the bar in *c* corresponds to 10 nm. The SiC nanorods shown in *a–c* were obtained from the reaction of carbon nanotubes with Si and I_2 at 1,200 °C for 2 h. The SiC nanorod shown in *d* was obtained from the reaction of nanotubes and SiO in a vacuum sealed quartz tube at 1,400 °C for 1 h. The NbC nanorods were obtained from the reaction of nanotubes with Nb and I_2 at 730 °C for 35 h.

The growth of TiC and SiC whiskers that have a crystalline, rod-like structure have been studied previously because these materials represent attractive reinforcing additives for metal and ceramic matrix composites[13–17]. The diameters of these whiskers have been typically >1,000 nm, although diameters as small as 100 nm have been observed. The carbide nanorods reported here have significantly smaller diameters, typically in the range 2–30 nm, and thus represent a major step in size reduction (comparable to the production of carbon nanotubes[5] compared with carbon fibres[18]). We are not aware of carbide whiskers analogous to the other carbide nanorods prepared in our studies (Table 1). Our data can be explained in part by a mechanism involving template-mediated growth, whereby carbon nanotubes define the diameter of the product carbide nanorods formed following reaction with a volatile species[10,11]. The similarity of the nanorod average diameters (and morphologies in the case of polycrystalline NbC) to that of the starting nanotubes is consistent with this proposal, but we cannot at present rule out contributions from catalytic growth and/or sintering of small tubes. Although a deeper understanding of the nanorod growth mechanism is clearly needed, we note that template-mediated growth could in principle produce carbide nanorods of any stable metal carbide.

We believe that these materials offer exciting opportunities for both fundamental research and technological applications. The wide range of nanorod properties and morphologies suggests that these materials may represent important building blocks for nanostructures. For instance, current flowing through our helical, metallic nanorods would lead to a modulated magnetic field that might be exploited for sensing or manipulation. The small diameters and range of chemical compositions available for these carbide nanorods could also make them useful as chemically specific reinforcements in metal and ceramic matrix composites, as well as perhaps an ideal structure with which to pin vortices in high-temperature superconductors. □

Received 30 March; accepted 23 May 1995.

1. Ruoff, R. S. *Nature* **372,** 731–732 (1994).
2. Guerret-Piecourt, C., Le Bouar, Y., Loiseau, A. & Pascard, H. *Nature* **372,** 761–764 (1994).
3. Tsang, S. C., Chen, Y. K., Harris, P. J. F. & Green, M. L. H. *Nature* **372,** 159–162 (1994).
4. Ajayan, P. M. & Iijima, S. *Nature* **361,** 333–334 (1993).
5. Seraphin, S., Zhou, D., Jiao, J., Whithers, J. C. & Loutfy, R. *Nature* **362,** 503 (1993).
6. Snyder, C. E. *et al. Int. Patent* WO 89/07163 (1989).
7. Iijima, S. *Nature* **354,** 56–58 (1991).
8. Ebbesen, T. W. & Ajayan, P. M. *Nature* **358,** 220–222 (1992).
9. Colbert, D. T. *et al. Science* **266,** 1218–1222 (1994).
10. Okada, K. & Nakajima, K. *Eur. Patent Applic.* EP 60388 A2 (1993).
11. Zhou, D. & Seraphin, S. *Chem. Phys. Lett.* **222,** 233–238 (1994).
12. Storms, E. K. *The Refractory Carbides* 1–17 (Academic, New York, 1967).
13. Wang, L., Wada, H. & Allard, L. F. *J. Mater. Res.* **7,** 148–163 (1992).
14. McMahon, G., Carpenter, G. J. C. & Malis, T. F. *J. Mater. Sci.* **26,** 5655–5663 (1991).
15. Verma, A. R. & Krishna, P. *Polymorphism and Polytypism in Crystals* (Wiley, New York, 1966).
16. Wokulski, Z. & Wokulska, K. *J. Cryst. Growth* **62,** 439–446 (1983).
17. Tamari, N. & Kato, A. *J. Cryst. Growth* **46,** 221–237 (1979).
18. Speck, J. S., Endo, M. & Dresselhaus, M. S. *J. Cryst. Growth* **94,** 834–848 (1989).
19. Lundstrom, T. in *Boron and Refractory Borides* (ed. Matkovich, V. I.) 351–376 (Springer, New York, 1977).

ACKNOWLEDGEMENTS. We thank Y. Liu and M. Frongillo for their help in obtaining the high-resolution TEM data. C.M.L. was supported by the MRSEC Program of the US NSF.

An efficient prebiotic synthesis of cytosine and uracil

Michael P. Robertson & Stanley L. Miller

Department of Chemistry and Biochemistry, University of California, San Diego, La Jolla, California 92093-0317, USA

In contrast to the purines[1–3], the routes that have been proposed for the prebiotic synthesis of pyrimidines from simple precursors give only low yields. Cytosine can be synthesized from cyanoacetylene and cyanate[4,5]; the former precursor is produced from a spark discharge in a CH_4/N_2 mixture[4,5] and is an abundant interstellar molecule[6]. But this reaction requires relatively high concentrations of cyanate (>0.1 M), which are unlikely to occur in aqueous media as cyanate is hydrolysed rapidly to CO_2 and NH_3. An alternative route that has been explored[7] is the reaction of cyanoacetaldehyde (formed by hydrolysis of cyanoacetylene[8]) with urea. But at low concentrations of urea, this reaction produces no detectable quantities of cytosine[7]. Here we show that in concentrated urea solution—such as might have been found in an evaporating lagoon or in pools on drying beaches on the early Earth—cyanoacetaldehyde reacts to form cytosine in yields of 30–50%, from which uracil can be formed by hydrolysis. These reactions provide a plausible route to the pyrimidine bases required in the RNA world[9].

The previous lack of plausible prebiotic syntheses of cytosine and uracil has led some authors to suggest that other bases were used in the first genetic material, such as the pyrimidines isocytosine and diaminopyrimidine[10], urazole and guanazole[11] and purines alone[12,13]. But the presence of pyrimidines in the Murchison meteorite at one-fifth the concentration of purines[14,15] suggests than an efficient prebiotic synthesis of pyrimidines should be possible. Ferris *et al.*[7] showed that cyanoacetaldehyde reacts with guanidine to produce diaminopyrimidine, but only with yields of 0.1–2%. Diaminopyrimidine can serve as a source of uracil by hydrolysis, but this provides only very low

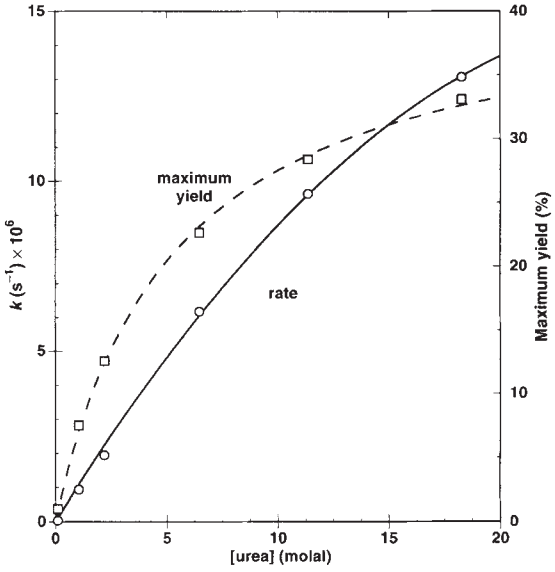

FIG 1 Rate constants and maximum yield for cytosine formation at 100 °C from cyanoacetaldehyde (10^{-3} M) and urea. These pseudo-first-order rate constants are based on the initial rates after 5 h. The maximum yield is the sum of cytosine and uracil which is formed by hydrolysis of cytosine (40% after 120 h). The cyanoacetaldehyde was prepared, from isoxazole (Aldrich) and the concentration determined spectrophotometrically using a molar absorptivity of 15,200 M^{-1} cm^{-1} at 248 nm for the anion[7]. The standard pyrimidines were obtained from Sigma. The HPLC analysis was performed with a Beckman model 110B HPLC system using a YMC ODS-AQ analytical reversed phase column and a Kratos absorbance detector set at 260 nm. The mobile phase was 0.1 M pH 4.8 sodium phosphate at 1 ml min^{-1}. The cytosine and uracil were identified by HPLC elution time, co-injection of a known sample, ultraviolet absorption spectra and proton NMR (GE 300 MHz).